nature portfolio

Peer Review File

# Ferromagnetism and correlated insulating states in monolayer $Mo_{33}Te_{56}$

Corresponding Author: Professor chendong zhang

**This file contains all reviewer reports in order by version, followed by all author rebuttals in order by version.**

Version 0:

Reviewer comments:

Reviewer #1

(Remarks to the Author)
I have read the manuscript by Pan et al. with great interest. This paper reports a novel material structure: the Mo33Te56 monolayer, synthesized by annealing the MoTe2 monolayer and featuring a periodic mirror-twin boundary loop superlattice. The experimental and theoretical results are of high quality and well consistent and found the Mo33Te56 monolayer possesses two sets of kagome bands lying near the Fermi level. This leads to pronounced and compelling correlated behaviors, including itinerant ferromagnetism and a correlated gap as large as 15meV at the EF. The search for kagome materials at the monolayer thickness is of practical interest, as it is crucial for manifesting the ideal 2D properties of kagome systems. Previous approaches, whether by top-down thinning of bulk crystals or utilizing molecular surface self-assembly, have not yet achieved the kagome electronic properties. Given these considerations, the present work is an exciting contribution to the fields of 2D materials and kagome research communities.
In my opinion, this paper merits publication in Nature Communications. However, before publication, there are a few issues that the authors should consider addressing.

1. The consistency between the STS spectral features and the calculated LDOS is quite good. However, there are some slight differences in certain fine features, such as the spectral weights and the wiggles. Would it be possible for the authors to provide an explanation for these discrepancies?
2. The authors have made a valuable attempt to provide an intuitive explanation of the kagome lattice, which I appreciate. It was pointed out that the center of the boundary forms a breathing kagome pattern. However, electrons do not seem to localize at those centers, even for P-1. Could the authors clarify how to construct lattices from these centers?
3. The kagome lattices are currently presented only in the supplementary materials. It might be helpful to also include the kagome grid in the main text for a more intuitive presentation.
4. Can the collapse of the correlation gap at 77 K be explained or expected? The gap energy scale is larger than this temperature scale.
5. The authors clearly define the gap size  0, but  N is not defined similarly. A clearer visual representation of  N is needed for better clarity.
6. As mentioned in this paper, the CT-kagome Mo5Te8 phase (Nat. Commun. 14, 6320 (2023)) is also prepared from single-layer H-MoTe2. Could the authors clarify the relationship and differences between Mo5Te8 and Mo33Te56 in terms of their preparation process? A more detailed description of the routes leading to the formation of the superstructures would be helpful.

Reviewer #2

(Remarks to the Author)
Dear Editor,
Z. Pan et al. report on the structural, electronic, and magnetic properties of a previously unreported stoichiometric phase of molybdenum telluride, Mo33Te56. The authors prepare the monolayer material upon bilayer graphene on SiC via molecular beam epitaxy and characterize the sample using scanning probe microscopy techniques complemented by density functional theory and tight-binding calculations. The authors demonstrate ferromagnetism and a correlated insulating gap at the Fermi energy.
Overall, this investigation into the correlated behaviour arising from the Kagome geometry of Mo33Te56 is an interesting and

thorough study in which the authors' claims are well supported by the data presented. We would be happy to recommend this work for publication if the authors are able to address the few comments listed below.
1. Could the authors provide more details on how the theoretical spin density plot shown in the lower part of Fig. 3c was produced (it does not appear in the Methods section currently)?
2. Are the nc-AFM measurements shown performed with the functionalization of the probe? Could the authors comment further on this in the methods section/SI?
3. The authors identify the stoichiometry largely by comparing experimental and simulated AFM images. However, this nc-AFM method lacks chemical resolution, and the authors should justify their identification of the stoichiometry further. From the AFM measurements performed, it would be interesting to know the differences in heights between the new Mo33Te56 phase and the BLG substrate. How does this height difference compare to previous reports of ML-MoTe2 (such as MoTe2 on WSe2 shown for comparison in Fig. S1e-f, for example)?
4. The experimental data shown for the SP-STM measurements in Fig. 3 (and related SI figures) appears very smooth. This may be due to the averaging process the authors allude to. However, given that the differences in spin polarisation are small, it would be good to see the raw experimental data shown with a clear explanation/demonstration of the averaging process in the SI for transparency.
5. Minor suggestion: it would be interesting to carry out spin-polarized DFT+U calculations, which can count better for e-e correlation than standard GGA PBE calculation at roughly similar computational cost.
6. In DFT simulations, was the graphene substrate considered? What is the interaction of MoTe layer with the substrate (see also Q3)?

Reviewer #3

(Remarks to the Author)
The paper reports the experimental realization of kagome physics in a new monolayer Mo-Te stoichiometric phase, Mo33Te56, synthesized through molecular beam epitaxy. It demonstrates the manifestation of both ferromagnetism and correlated insulating states. The authors employed a combination of experimental techniques (MBE, STM, SP-STM, AFM, etc.) alongside theoretical methods (DFT, TB, group theoretical analysis, etc.). The results are coherent and well-aligned, showing an innovative and robust approach to constructing novel kagome structure within atomically thin van der Waals materials. I believe this paper is worthy of consideration for publication in Nature Communications. There are some minor comments:
(1) Fig. 1b&c exhibits chiral "wagon-wheel-like" structures, whereas the kagome lattice is typically characterized by in-plane mirror symmetry. How can these chiral structures be reconciled with the kagome lattice framework? Could the authors provide a more schematic explanation to clarify this?
(2) The authors provide a fairly comprehensive analysis of the gap formation mechanism at the Fermi level, particularly in their exclusion of specific manifestations of a Coulomb gap, such as V-shaped gaps or those arising from Coulomb blockade. However, it is worth noting that the possibility of a Coulomb gap could persist in the absence of these effects. For example, previous studies have shown that U-shaped gaps can emerge due to tunneling into Landau levels, which are a characteristic signature of topologically flat bands, independent of band filling [Phys. Rev. Lett. 69, 3804–3807 (1992); Nature 464, 566–570 (2010)]. It might be beneficial for the authors to consider these potential scenarios in their analysis.
(3) The gap size mentioned in the manuscript is 15 mV. How was this value determined from the tunneling spectra? Was spatial variation taken into account when reporting this number? If it's a statistical average, an error bar should be included.
(4) The authors mention that the Mo33Te56 phase is uniform across nearly the entire sample. It would be better if additional evidence could be provided to support this claim.
(5) In Fig. S5e, the dI/dV spectra show the in-gap states for N = 3, 4, 5. Are there any further experimental/theoretical investigations on the morphology and electronic structure of these states? Do they still exhibit the kagome band properties?
(6) The authors should consider adding graphical representations to make the kagome lattice more visually intuitive and comprehensible.
(7) In Fig. 4a, the caption “TDA/B” should be revise to “TDE/U” for consistency with the manuscript.

Reviewer #4

(Remarks to the Author)
I co-reviewed this manuscript with one of the reviewers who provided the listed reports. This is part of the Nature Communications initiative to facilitate training in peer review and to provide appropriate recognition for Early Career Researchers who co-review manuscripts.

Version 1:

Reviewer comments:

Reviewer #1

(Remarks to the Author)
In this revised manuscript, the authors have properly addressed all the concerns and suggestions rasied by the referees. I thus, believe the manuscript is now acceptable in the present form.

Reviewer #2

(Remarks to the Author)
No more comments,I agree on publishing the manuscript.

Reviewer #3

(Remarks to the Author)
The authors have answered all of the comments very well, I think it can be accepted for publishing. Before that, a few minor issues need to be considered.
1. In page 6 line 142, the author claim "In contrast, the present pattern exhibits uniformity across nearly the entire sample.". Since STM and AFM characterization is locally in a small region, such claim is a little bite of over optimistic，unless the author present some evidence from macroscopic measurement, such as LEED pattern. And also such Mo33Te56 phase is special stoichiometric Mo-Te compounds that form via an annealing process of the single-layer H-MoTe2, I doubt it can be uniformly cover the entire sample. I suggest the author tune down a little.
2. In figure 1g caption, they state "the dI/dV spectra are normalized by the total conductance (I/V) to mitigate the influence of bias-dependent tunneling probability on the spectral weight." So all STS panels should be lableled as "(dI/dV)/(I/V)", instead of "normalized dI/dV" or "dI/dV".please correct it.
3. Although the author use a large paragraph in Supplementary Information (SI) to describe how "The array of MTB loop triangles forms a breathing colouring-triangle pattern.", it is still hard to see the Kagome structure. I suggest the author can draw accordingly the Kagome lattice in Fig. 1 or Fig. 2.

Reviewer #4

(Remarks to the Author)
I co-reviewed this manuscript with one of the reviewers who provided the listed reports. This is part of the Nature Communications initiative to facilitate training in peer review and to provide appropriate recognition for Early Career Researchers who co-review manuscripts.

# Point-by-point responses to reviewer comments

Manuscript ID: NCOMMS-24-78805

Title: "*Ferromagnetism and correlated insulating states in monolayer $Mo_{33}Te_{56}$*"

*Reviewer #1 (Remarks to the Author):*

***Comment 1-0.*** *I have read the manuscript by Pan et al. with great interest. This paper reports a novel material structure: the $Mo_{33}Te_{56}$ monolayer, synthesized by annealing the $MoTe_2$ monolayer and featuring a periodic mirror-twin boundary loop superlattice. The experimental and theoretical results are of high quality and well consistent and found the $Mo_{33}Te_{56}$ monolayer possesses two sets of kagome bands lying near the Fermi level. This leads to pronounced and compelling correlated behaviors, including itinerant ferromagnetism and a correlated gap as large as 15meV at the $E_F$. The search for kagome materials at the monolayer thickness is of practical interest, as it is crucial for manifesting the ideal 2D properties of kagome systems. Previous approaches, whether by top-down thinning of bulk crystals or utilizing molecular surface self-assembly, have not yet achieved the kagome electronic properties. Given these considerations, the present work is an exciting contribution to the fields of 2D materials and kagome research communities.*

*In my opinion, this paper merits publication in Nature Communications. However, before publication, there are a few issues that the authors should consider addressing.*

**Response 1-0:** We sincerely appreciate the Reviewer's thorough evaluation, valuable comments, and positive recommendation. His/her comments have been well addressed in the following point-to-point responses.

***Comment 1-1.*** *The consistency between the STS spectral features and the calculated LDOS is quite good. However, there are some slight differences in certain fine features, such as the spectral weights and the wiggles. Would it be possible for the authors to provide an explanation for these discrepancies?*

**Response 1-1:** We thank the Reviewer for raising this concern. In scanning tunneling spectroscopy, the spectral weight is influenced by many factors during the tunneling process (as we will elucidate in the following). This indeed presents limitations in accurately reflecting the magnitude of the density of states (DOS), especially when compared to measurements of energy levels and spatial distributions.

(1) The relative spectral weights in scanning tunneling spectroscopy, particularly on a large energy scale, were known to deviate from the actual situation. The assumption that the measured d$I$/d$V$ is proportional to the sample DOS is based on the approximation that the tunneling matrix and the tip DOS are constant (*i.e.*, $V$ independent). In a realistic measurement, in addition to the unmanageable tip DOS over a large energy scale, the tunneling matrix is certainly bias-dependent (since the geometry of the tunneling barrier is regulated by the tip-sample bias [*Rev. Mod. Phys.* **79**, 353 (2007)]. In addition, the parallel moment ($k_{\|}$) of sample states also plays a significant role in the effective tunneling decay constant $\kappa$ (in a simplified model $\kappa \approx \sqrt{\frac{2m\Phi_b + k_{\|}^2}{\hbar^2}}$), which has been known to influence the signal intensity in STS detection [*Phys. Rev. Lett.* **50**, 1998–2001 (1983); *Phys. Rev. B* **31**, 805–813 (1985); *Nano Lett.* **15**, 6494–6500 (2015)].

Another discrepancy between the experimental spectrum and the DFT DOS profile is that the experimental spectrum reflects the very local DOS, while the theoretical DOS is an integration over a unit cell. In the manuscript, we use a simple numerical average of the four spectra taken at four typical sites and the corresponding average spectrum, which is certainly not a strict reproduction of the spatial integration.

(2) The wiggles in the DFT DOS (bottom panel of Fig. 1h) have a magnitude of ~ 40 meV, which does not affect the general consistency in the primary line shapes with the experiments. The experimental spectra in Fig. 1h contain many sources of signal broadening, including the lock-in modulation voltage $V_{\mathrm{rms}}$ (7 mV here), instrumental broadening (*e.g.,* radio frequency noise with $T_{\mathrm{eff}}$ ~ 2 K in our measurements), and smoothing used in data processing (10-point Savitzky–Golay with a point increment of ~ 1 mV). Thus, the total broadening $\Delta E \sim \sqrt{(2eV_{rms})^2 + (3.5k_BT)^2 + (3.5k_BT_{eff})^2 + \Delta E_{smooth}} \sim$

18 meV is comparable to the wiggles' energy scale. In addition, some subtle interactions, such as long-range *e-e* interaction, which have not been well included in the DFT+*U* calculation, may also reshape the DOS on the energy scale of a few to tens of meV.

***Comment 1-2.*** *The authors have made a valuable attempt to provide an intuitive explanation of the kagome lattice, which I appreciate. It was pointed out that the center of the boundary forms a breathing kagome pattern. However, electrons do not seem to localize at those centers, even for* $P_{-1}$*. Could the authors clarify how to construct lattices from these centers?*

**Response 1-2:** We thank the Reviewer for raising this concern. As demonstrated by rigorous irreducible representation analysis, the kagome symmetry is a well-established feature of the $Mo_{33}Te_{56}$ structure. In the original submission, we employed a line graph representation of the boundary network to provide a simple and easily understandable schematic illustration in real space. In reality, there are other equally valid intuitive representations. For instance, the MTB loop triangles (*i.e.*, the red lines in Fig. R1a) are arranged in an array, which itself forms a breathing, colouring-triangle pattern. Both examples qualitatively demonstrate the kagome geometry of the atomic structure in real space.

Regarding a more practical depiction of the kagome pattern based on electronic structures, there are two aspects that differ from atomic kagome materials. First, we observe multiple sets of kagome bands in this system, each corresponding to different real-space distributions of electronic states at various energy levels. Second, for any specific set of kagome bands, the electron density cannot be entirely localized at a single point, unlike in atomic kagome materials where lattice points are clearly defined. A straightforward approach is to select the locations with maximum DOS as the lattice points. Following this approach, we can also draw a kagome pattern for the $P_{-1}$. As shown in Fig. R1b and 1c, the DOS distribution at the boundary is not uniform; it is strongest at one end, specifically at the three triangularly arranged spots near the central region (marked in Fig. R1b). By adjusting the colour scale of the image, we can visually

highlight a breathing, tilted kagome pattern (Fig. R1c).

In terms of tight-binding (TB) fitting, there is a degree of flexibility in lattice site selection that does not affect the main conclusions. The lattice sites need not align with the maximum DOS locations. Instead, we take a more general approach by first creating a standard kagome lattice in real space (as shown by the black grid in Fig. S8 (R1d) with the lattice site near the boundary centre). From this standard structure, we obtain the breathing pattern ($t_a \neq t_p$) by fitting the hopping parameters. This method, grounded in the atomic structure's symmetry, effectively captures the essential features of the electronic kagome pattern. It is a rational and effective strategy.

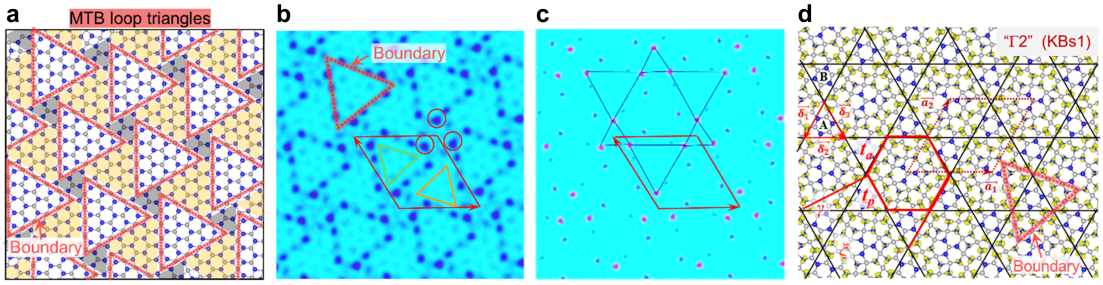


**Fig. R1. a**, The array of MTB loop triangles forms a breathing colouring-triangle pattern. **b**, Simulated d$I$/d$V$ maps for $P_{-1}$ (as shown in Fig. 2c), where the spots with the largest DOS are marked by red circles. **c**, The same map as in (**b**) with a rescaled colour scale to highlight the spots with the strongest DOS. The strongest DOS points suggest the formation of a breathing, tilted kagome lattice (blue lines). **d**, The tight-binding model used in Fig. S8.

**Action 1-2:** In the resubmitted files, we have provided a detailed discussion to clarify the construction of the kagome lattices in our system [lines 214–215, page 9 in the main text; lines 288–297, pages 17–18 in Supplementary Information (SI)].

***Comment 1-3.*** *The kagome lattices are currently presented only in the supplementary materials. It might be helpful to also include the kagome grid in the main text for a more intuitive presentation.*

**Response & Action 1-3:** We thank the Reviewer for this suggestion. We have depicted the kagome grid in the revised Fig. 2c with the lattice points at the boundary centre (lines 214–215, page 9 in the main text). As discussed in Response 1-2, this is intended as a straightforward and clear schematic representation of the kagome geometry in real

space. More detailed discussions have been added to the SI in this revision (lines 288–297, pages 17–18).

***Comment 1-4.*** *Can the collapse of the correlation gap at 77 K be explained or expected? The gap energy scale is larger than this temperature scale.*

**Response 1-4:** One of the characteristics of a correlation gap is that its collapse cannot be solely depicted by the thermal broadening governed by the Fermi–Dirac distribution. Mathematically, the thermal smearing effect can be depicted as convoluting the differential conductivity with the derivative of the Fermi–Dirac distribution, as follows:

$$\frac{dI}{dV}(eV) \propto \int_{-\infty}^{\infty} \rho(E) \left( \frac{d}{dV} F(E - eV, T) \right) \mathrm{d}E$$

where $\rho(E)$ is the zero-temperature density of states and $F(E,T) = \frac{1}{1+\exp(\frac{E-\mu}{k_B T})}$ is the Fermi–Dirac distribution, with $\mu$ being the chemical potential. The full width at half-maximum (FWHM) of the thermal smearing is proportional to 3.5 $k_B T$. Therefore, the measuring temperature $T$ = 77 K corresponds to a thermal broadening of 23 meV (and 3.5 meV for $T$ = 12 K).

In our experiment, the gap at 0.35 K with a magnitude of ~ 15 meV gets closed at 12 K (*i.e.*, the zero-conductance region disappears). Such suppression is much faster than a pure thermal broadening effect, evidencing the correlation nature of the observed gap. In the main text, Fig. 4c and 4d show mathematical simulations for $T$-dependent thermal smearing, illustrating the above conclusion.

***Comment 1-5.*** *The authors clearly define the gap size $\Delta_0$, but $\Delta_N$ is not defined similarly. A clearer visual representation of $\Delta_N$ is needed for better clarity.*

**Response & Action 1-5:** We thank the Reviewer for his/her careful review and for raising this issue. We acknowledge that the definition of $\Delta_N$ was not sufficiently clear, and we apologize for this oversight The magnitude of $\Delta_N$ is determined by the separations between the maximum points in the $|\mathrm{d}^2I/\mathrm{d}V^2|$ spectra, which corresponds to

the midpoints of the edge slopes. In this revision, we clarified the determination of $\Delta_N$ by adding a new supplementary figure (Fig. S18a, also referenced in Fig. R2). The corresponding discussions were added in the SI (lines 534–536, page 33).

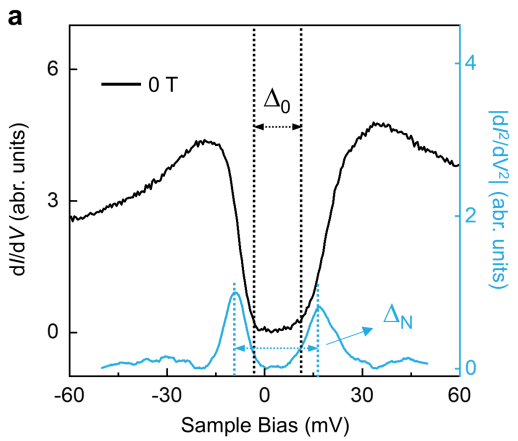


**Fig. R2.** Determination of $\Delta_0$ and $\Delta_N$. Tunnelling spectra obtained with a W tip at 0 T. The gap size $\Delta_0$ (black dashed lines) defines the energy range of the zero-conductance region. The gap size $\Delta_N$ (blue dashed lines) is determined by the midpoints of the edge slopes, *i.e.*, the maximum point in the $|d^2I/dV^2|$ spectra.

***Comment 1-6.*** *As mentioned in this paper, the CT-kagome $Mo_5Te_8$ phase (Nat. Commun. 14, 6320 (2023)) is also prepared from single-layer H-$MoTe_2$. Could the authors clarify the relationship and differences between $Mo_5Te_8$ and $Mo_{33}Te_{56}$ in terms of their preparation process? A more detailed description of the routes leading to the formation of the superstructures would be helpful.*

**Response 1-6:** We thank the Reviewer for raising this concern. Both $Mo_5Te_8$ and $Mo_{33}Te_{56}$ are special stoichiometric Mo-Te compounds that form *via* an annealing process of the single-layer H-$MoTe_2$, with the formation of mirror twin boundaries (MTBs) playing a critical role in their structural evolution. However, there are key differences in the preparation routes that lead to distinct superstructures:

As reported in [*Nat. Commun.* **14**, 6320 (2023)], the $Mo_5Te_8$ phase was grown on a highly oriented pyrolytic graphite (HOPG) substrate, with deposition occurring at approximately 240 °C, followed by annealing at 340 °C. The observed $Mo_5Te_8$ phase is characterized by small domains, typically concentrated in island structures, and is

often mixed with other Mo-Te phases. It is important to note that the formation of transition metal dichalcogenide (TMD) thin films via MBE can be influenced by several factors, such as the choice of substrate, substrate temperature, flux ratios, and the method of substrate heating. These factors can significantly affect the final structure. Thus, it is inappropriate to directly compare the parameters given in the literature to the $Mo_{33}Te_{56}$ phase in our study. To address this, we have systematically investigated and characterized both $Mo_5Te_8$ and $Mo_{33}Te_{56}$ under carefully controlled settings, enabling us to conduct a comprehensive analysis of their relationship and differences.

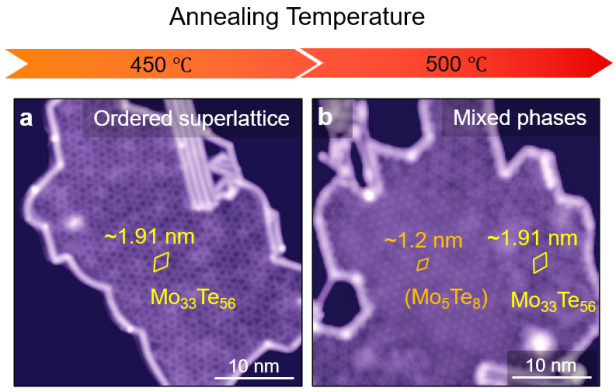


**Fig. R3. a**, Ordered MTB superlattice with a uniform periodicity of ~1.91 nm, *i.e.*, the $Mo_{33}Te_{56}$ phase (marked by yellow lines). **b**, Two distinguishable regions: one possesses hexagonal symmetry with an ~1.2 nm superlattice periodicity, which corresponds to the $Mo_5Te_8$ phase (marked by orange lines); the other is identified as the $Mo_{33}Te_{56}$ phase. During the annealing process, $Mo_6Te_6$ wires appear at the very edge of the sample flakes. Scanning parameters: (a) bias voltage $V_{bias}$ = 2 V, tunnelling current $I_t$ = 20 pA; (b) 1 V, 20 pA.

Our findings show that one of the primary differences between the two phases lies in the annealing temperatures. $Mo_5Te_8$ is obtained by annealing at a higher annealing temperature (500 °C, Fig. R3b) compared to $Mo_{33}Te_{56}$ (450 °C, Fig. R3a), which results in greater Te desorption and a lower Te: Mo stoichiometric ratio. In addition, in our growth preparation work, the $Mo_{33}Te_{56}$ phase can be effectively isolated from other phases in the growth parameter space, whereas the $Mo_5Te_8$ phase is always mixed with other phases ($Mo_{33}Te_{56}$ and $Mo_6Te_6$) and shows a limited coverage percentage, as summarized in Table R1. Detailed insights into the synthesis routes can be found in our recent work which thoroughly discusses the technical aspects of material growth [*Appl. Phys. Lett.* **125**, 151601 (2024)]. Additionally, we have computed and compared the

band structures of both phases, providing a detailed analysis of the electronic properties and the differences between $Mo_{33}Te_{56}$ and $Mo_5Te_8$ [*arXiv:* 2408.14285].

| | Annealing Temperature | morphology | periodicity | coverage |
|---|---|---|---|---|
| $Mo_{33}Te_{56}$ | 450 ℃ | Wagon wheel pattern | ~1.91 nm | Dominant |
| $Mo_5Te_8$ | 500 ℃ | hexagonal arrays | ~1.2 nm | Limited |

**Table R1. The comparison between the $Mo_5Te_8$ and $Mo_{33}Te_{56}$ phases.**

*Reviewer #2 (Remarks to the Author):*

***Comment 2-0.*** *Z. Pan et al. report on the structural, electronic, and magnetic properties of a previously unreported stoichiometric phase of molybdenum telluride, $Mo_{33}Te_{56}$. The authors prepare the monolayer material upon bilayer graphene on SiC via molecular beam epitaxy and characterize the sample using scanning probe microscopy techniques complemented by density functional theory and tight-binding calculations. The authors demonstrate ferromagnetism and a correlated insulating gap at the Fermi energy.*

*Overall, this investigation into the correlated behaviour arising from the Kagome geometry of $Mo_{33}Te_{56}$ is an interesting and thorough study in which the authors' claims are well supported by the data presented. We would be happy to recommend this work for publication if the authors are able to address the few comments listed below.*

**Response 2-0:** We thank the Reviewer for his/her careful review, constructive comments, and positive recommendation. His/her comments have been well addressed in the following point-to-point responses.

***Comment 2-1.*** *Could the authors provide more details on how the theoretical spin density plot shown in the lower part of Fig. 3c was produced (it does not appear in the Methods section currently)?*

**Response 2-1:** We greatly appreciate the Reviewer for this constructive comment. We apologize for the oversight in the Methods section. The spin DOS plot shown in the lower part of Fig. 3c and Fig. S11 was derived from the difference between the spin-up and spin-down density of states using the definition of $N_{\mathrm{spin}}(E) = N_{\mathrm{spin-up}}(E) - N_{\mathrm{spin-down}}(E)$, where $N$ is the spin-resolved density of states and $E$ is the energy level.

**Action 2-1:** In the resubmitted files, we have included the relevant details regarding the calculation of the theoretical spin DOS plot in the Methods section, with the sentence: "The spin DOS was calculated using $N_{\mathrm{spin}}(E) = N_{\mathrm{spin-up}}(E) - N_{\mathrm{spin-down}}(E)$." (lines 397–398, page 19 in the main text). Furthermore, we have thoroughly revised the Methods section pertaining to the DFT calculations, ensuring the inclusion of all

essential technical details (lines 392–408, pages 19–20 in the main text). This systematic update not only improves clarity but also facilitates the reproducibility of the calculations presented in this study.

***Comment 2-2.*** *Are the nc-AFM measurements shown performed with the functionalization of the probe? Could the authors comment further on this in the methods section/SI?*

**Response & Action 2-2:** We thank the Reviewer for raising this concern. We apologize for not explicitly clarifying the AFM probe details in the original manuscript. In our study, the nc-AFM measurements were carried out using a standard tungsten (W) tip, a widely adopted method for achieving atomic-scale resolution in imaging inorganic crystalline materials [*Nat. Commun.* **10**, 2847 (2019); *Nat. Commun.* **11**, 5613 (2020)].

Probes functionalized with molecules or atoms are indeed a powerful technique for enhancing imaging sensitivity and hold significant value in the study of chemical bonds within organic molecular systems. For the primary focus of our work—resolving the atomic structure of the $Mo_{33}Te_{56}$ surface—the use of a functionalized probe was not necessary. The unmodified probe offered sufficient sensitivity for high-resolution atomic imaging of the surface features.

To clarify this point, we have updated the Methods section in the revised manuscript with the following statement: "*The nc-AFM measurements were performed using a standard W tip.*" (line 377, page 18 in the main text).

***Comment 2-3.*** *The authors identify the stoichiometry largely by comparing experimental and simulated AFM images. However, this nc-AFM method lacks chemical resolution, and the authors should justify their identification of the stoichiometry further. From the AFM measurements performed, it would be interesting to know the differences in heights between the new $Mo_{33}Te_{56}$ phase and the BLG substrate. How does this height difference compare to previous reports of ML-$MoTe_2$ (such as $MoTe_2$ on $WSe_2$ shown for comparison in Fig. S1e-f, for example)?*

**Response 2-3:** We appreciate the Reviewer's valuable comments and concerns. In the following, we address both the identification of stoichiometry and the height differences between the $Mo_{33}Te_{56}$ phase and the BLG substrate.

1) Regarding the identification of stoichiometry, it essentially involves determining the atomic structure. To address this, we follow a standard methodology commonly used in STM studies of low-dimensional material structures, as we will explain step by step below.

• Our scanning probe measurements (Fig. R4a) display that the as-grown superlattice exhibits a "wagon-wheel" pattern, whose size and concentration are thermally dependent. This pattern is a well-known hallmark of the mirror twin boundary (MTB) network structure. The MTB itself has a well-established structural model where the row of chalcogen atoms is centred along the boundary and each chalcogen atom is bound to four metal atoms instead of three. In our work, the $Mo_{33}Te_{56}$ superlattice exhibits a periodicity of 1.91 nm. The atomic-resolution AFM measurement further reveals that the triangular domain consists of six surface Te atoms (*i.e.*, three Mo-Te units), with an interatomic distance of 0.365 nm (Fig. R4a, right panel). These findings enable an accurate determination of the atomic structure of the boundary and domain. However, regarding the structure at the centre of the "wagon-wheel" network, there remain uncertainties in the literature lie in the number of Mo vacancies. Depending on the specific fabrication process and the domain size, previous studies have proposed various configurations, including no Mo vacancies, three Mo vacancies, and six Mo vacancies [*ACS Nano* **11**, 11005–11014 (2017); *Nat. Commun.* **8**, 14231 (2017); *Nat. Commun.* **10**, 2847 (2019)].

• Determining which of these three configurations best represents the observed structure is the central issue in confirming the stoichiometry. Experimentally, one of the most prominent features for identifying the presence of Mo vacancies is the distinct contrast at the central region of the "wagon-wheel" pattern, as observed in AFM images. For example, in Fig. R4b [*Nat. Commun.* **10**, 2847 (2019)], three out of six Te hollow sites at the centre appear significantly darker than the surrounding positions (also using

a standard W tip), a feature attributed to the presence of Mo vacancies. In our AFM experiments, we did not observe similar prominent contrast variations at the central region. This observation strongly suggests that the structure we obtained does not contain Mo vacancies. The simulated frequency-shift AFM image based on the no-Mo-vacancies model closely resembles this experimental feature (as shown in the original manuscript Fig. 1d and e).

• To understand this experimental observation and further validate the atomic model, we performed a theoretical comparison of the formation energies of three possible structural models as a function of the Te chemical potential, aiming to comprehensively simulate the experimental growth conditions (Fig. R4c-f). Our calculations reveal that, for the observed superlattice size, the model without Mo vacancies (Fig. R4c) exhibits significantly lower formation energies than the other two models (as depicted by the red curve versus the black & blue curves). In addition, the consistencies established between our theoretical predictions and experimental observations, particularly regarding the energy-dependent d$I$/d$V$ spectra (original Fig. 1h), further provide robust support for the validity of our proposed model.

• Finally, based on this model, we determined the stoichiometry of the new phase by counting the number of Mo and Te atoms in the unit cell (Fig. R4c). This analysis reveals 33 Mo atoms and 56 Te atoms per unit cell, identifying the stoichiometry as $Mo_{33}Te_{56}$.

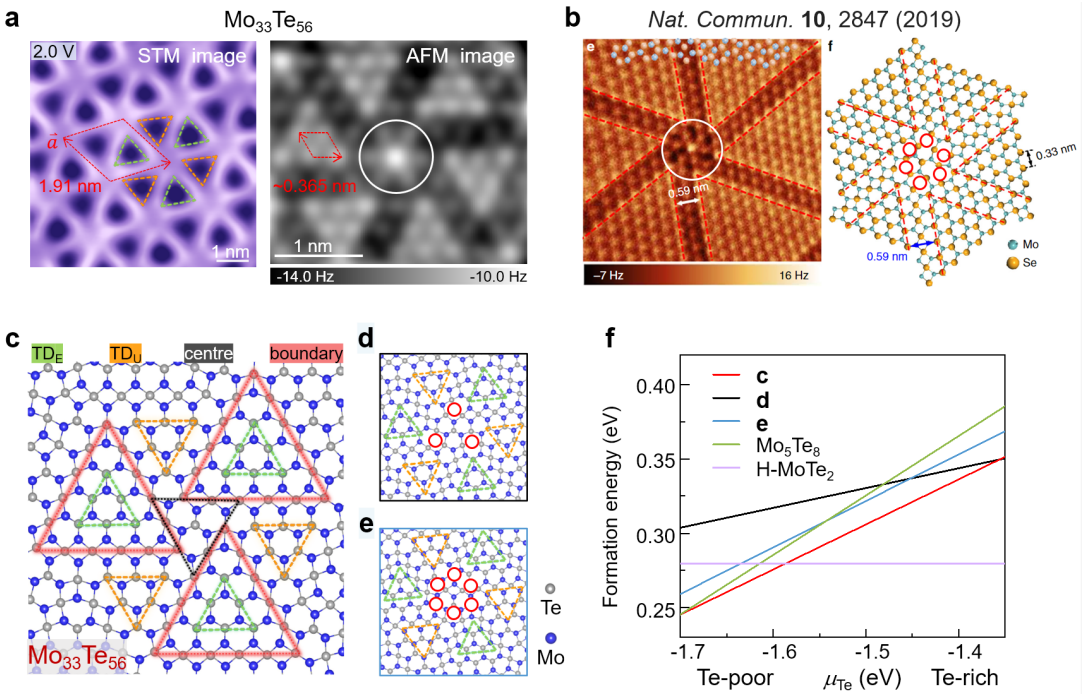


**Fig. R4. a**, STM (left) and AFM (right) images. The $Mo_{33}Te_{56}$ phase supercell is outlined by a red rhombus with a lattice constant of 1.91 nm (left), and the triangular domain, consisting of six surface Te atoms, exhibits an interatomic distance of 0.365 nm (right). **b**, AFM image and corresponding six-Mo vacancies model adapted from [*Nat. Commun.* **10**, 2847 (2019)]. The central regions are marked by white circles in both AFM images. **c-e**, Atomic models corresponding to the three structural possibilities: no Mo vacancy (**c**), three Mo vacancies (**d**), and six Mo vacancies (**e**). **f**, Formation energy compassion of the three models, showing the no-Mo-vacancy model (red) is the most thermodynamically stable.

2) Regarding the height differences, we did not measure the island heights directly using AFM. Our standard procedure involves using the STM mode for wide-area scans to locate suitable regions and avoid tip damage. Once regions of interest are identified, we switch to AFM mode for atomically resolved measurements. As a result, we do not have AFM-derived island height data and therefore rely on STM data for discussing the height difference. In the study of epitaxial two-dimensional materials, STM is also commonly utilized to measure the height of sample islands. It is known that relatively reliable height measurements are typically conducted under high bias voltages to minimize the influence of any local DOS maxima. In our subsequent discussion, we adhere to this criterion, with all height data derived from STM measurements conducted at a bias voltage of +2.0 V.

In Fig. R5, we present the STM measurements of the height difference between the $Mo_{33}Te_{56}$ phase and the underlying BLG (bilayer graphene) substrate, which is

approximately 0.81 nm (red curve in Fig. R5d). For the ML-$MoTe_2$ phase, the height difference is measured to be 0.82 nm (blue curve in Fig. R5d). This value is consistent with previous reports for monolayer $MoTe_2$ on BLG, which is typically slightly greater than 0.8 nm [*Nano Lett.* **18**, 675−681 (2018); *Chinese Phys. Lett.* **35**, 066801 (2018); *ACS Nano* **11**, 3282−3288 (2018)]. This consistency further supports the reliability of our STM height measurements.

When the substrate is replaced with $WSe_2$, the height of the $Mo_{33}Te_{56}$ phase is slightly reduced to approximately 0.76 nm [grey curve in Fig. R5d (now in Fig. S2g)]. Since the pure $MoTe_2$ phase was not intentionally grown on $WSe_2$ substrates, corresponding height data are not available. Given the differing chemical potentials of substrates, such minor variations in height between the BLG and $WSe_2$ substrates fall within the range of expected experimental results. Similar height variations, on the order of tens of picometers, have been reported for monolayer TMDs grown on various substrates [*ACS Nano* **12**, 7562−7570 (2018); *New J. Phys.* **17**, 053023 (2015)].

Our experiments reveal that the heights of $Mo_{33}Te_{56}$ and $MoTe_2$ are nearly identical. This observation can be further understood through theoretical structural models of the two materials. As shown in the side-view structural models in Fig. R5e (Fig. S2h), the presence of MTBs in $Mo_{33}Te_{56}$ induces slight corrugation in the *z*-direction. However, the overall thickness of $Mo_{33}Te_{56}$ shall not differ significantly from that of $MoTe_2$. Specifically, when measuring the distance between the centres of the top-layer and bottom-layer Te atoms, we obtain an average value of 0.364 nm (with the maximum and minimum distance ranging from ~0.405 nm to ~0.348 nm) for ML-$Mo_{33}Te_{56}$, and 0.362 nm for ML-$MoTe_2$, highlighting the minor thickness differences between the two phases.

In conclusion, we hope this explanation clarifies the concerns raised and provides a more comprehensive understanding of our experimental results.

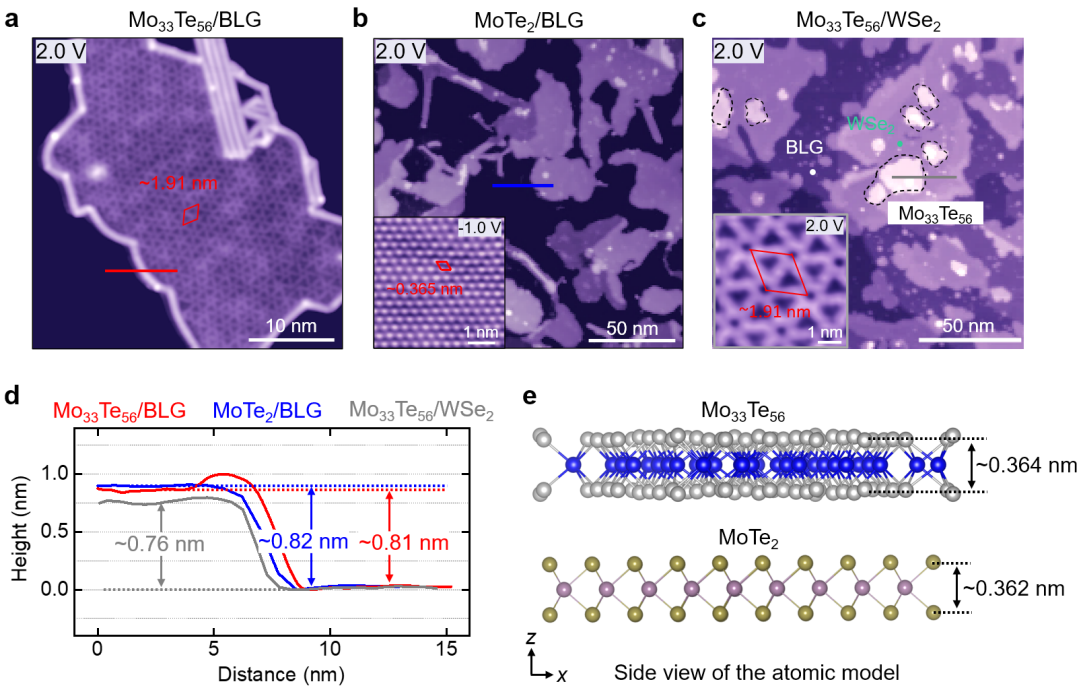


**Fig. R5. a-c**, STM images of $Mo_{33}Te_{56}$/BLG, $MoTe_2$/BLG, and $Mo_{33}Te_{56}/WSe_2$. **d**, Height profiles along the pathway indicated in (**a-c**). In the red curve, the slightly elevated bump near the edge of the island is attributed to the formation of one-dimensional $Mo_6Te_6$ nanowires. **e**, Side views of theoretical models of $Mo_{33}Te_{56}$ and $MoTe_2$. The distance between the centres of top- and bottom-layer Te atoms is labelled as shown.

**Action 2-3:** 1) In the resubmitted files, we have added a detailed discussion on the identification of the stoichiometry of the $Mo_{33}Te_{56}$ phase (lines 146–147, page 6 in the main text; lines 101–139, pages 7–9 in SI).

2) We have added the height of the $Mo_{33}Te_{56}$ phase in Fig. 1a, along with the corresponding discussion (see lines 88–90, page 4 in the main text; further details provided in lines 56–81, pages 4–5 in the SI).

***Comment 2-4.*** *The experimental data shown for the SP-STM measurements in Fig. 3 (and related SI figures) appears very smooth. This may be due to the averaging process the authors allude to. However, given that the differences in spin polarisation are small, it would be good to see the raw experimental data shown with a clear explanation/demonstration of the averaging process in the SI for transparency.*

**Response 2-4:** We thank the Reviewer for the insightful comments. We would like to

address these points in detail as follows:

1. In SP-STM measurements, the total polarization ($P$) in the measured d$I$/d$V$ is given by $P_{total} = P_{tip} \times P_{sample}$. As a result, $P_{total}$ is generally low, often being less than 10%. Therefore, confirming the reliability and authenticity of such subtle signal variations is one of the primary missions in SP-STM measurements. Here, we wish to emphasize two key points:

1) In the original Fig. 3b, the spectra under different magnetic fields appear to have a high degree of overlap and show minimal differences (*i.e.*, $P_{total}$ appears to be very small). This is primarily because the spectra are plotted over a relatively wide bias range. In Fig. R6a, we have re-plotted the data over a narrower bias range (*e.g.*, -0.05 V to -0.25 V). The spin polarization differences become more apparent and are clearly visible, and the magnitude of these variations is consistent with what is generally observed in the SP-STM field.

2) On the technical front of SP-STM measurements, the most effective method to confirm subtle magnetic field-dependent signal variations is by repeatedly switching between positive and negative magnetic fields to check the reproducibility of the changes. We have carefully verified this in our tests, as illustrated in Fig. 3d and 3e (also in original Fig. S10). In Fig. R6b, we have replotted a set of data obtained from "back-and-forth" magnetic field switching. It is evident that the differences in the spectra at +0.15 T and -0.15 T are reproducible and reliable.

2. The spectra presented in the main text have indeed undergone smoothing and averaging processes. Below, we provide a detailed explanation of the data processing procedures.

• **Multiple sweeps and averaging:** In our experiments, each raw spectrum is obtained by averaging multiple sweeps performed under identical parameters, typically with more than ten sweeps. In Fig. R6c, we display all the individual sweeps and the corresponding averaged spectra at three different magnetic fields (+0.5 T, -0.5 T, 0 T). This averaging process enhances the signal-to-noise ratio and leads to the smooth appearance of the raw data.

•**Normalization**: The raw d*I*/d*V* spectra are normalized by the total conductance (*I*/*V*) to eliminate the influence of bias-dependent tunneling probability on the spectral weight [*Phys. Rev. Lett.* **57**, 2579 (1986); *Am. J. Phys* **62**, 573–574 (1994)]. The total conductance (*I*/*V*) is also averaged in the same manner as described above. This approach is commonly employed in STS data processing to achieve better consistency with the theoretical DOS(*E*).

•**Smoothing**: To further improve data quality, the normalized spectra were smoothed using a 15-point Savitzky–Golay filter with a smoothing window of 10 mV. This process preserves the main features of the spectra while reducing noise.

•**Spatial averaging:** The spectrum in Fig. 3b is the average of the four spectra from Fig. S12a, obtained from all four typical sites and processed according to the procedures described above. A straightforward numerical averaging was employed here, without considering the weighting of different spatial locations.

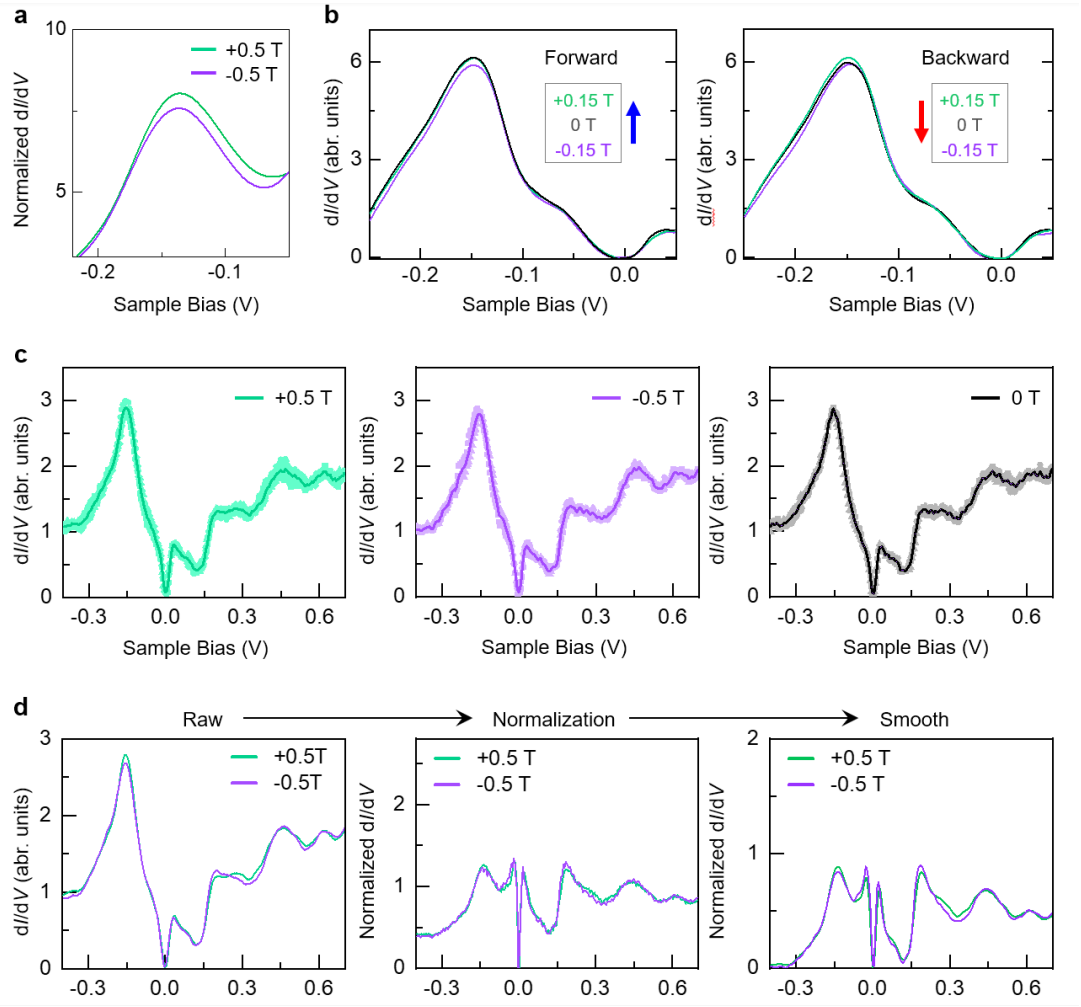

**Fig. R6. a**, Zoomed-in plot of Fig. 3b (-0.05 V to -0.25 V) highlighting the apparent differences due to spin polarization. **b**, Plot of the same dataset from Fig. 3d with a modified axis range, demonstrating the reproducibility and reliability of the spectral differences at +0.15 T and -0.15 T by examining "back-and-forth" magnetic field switching. **c**, Raw data at three magnetic fields (+0.5 T, -0.5 T, 0 T), including individual sweeps (shaded areas) and the averaged spectra (solid lines). **d**, Left panel is the average spectra from (**c**), normalized by total conductance (*I*/*V*) and smoothed using a 15-point Savitzky–Golay filter with a smoothing window of 10 mV. The boundary site serves as an example here. The right panel in (**d**) corresponds to the boundary panel in Fig. S12a.

**Action 2-4:** In compliance with the Reviewer's suggestion, we have included a detailed description of the data processing steps—including averaging, normalization, and smoothing procedures—in the supplementary information (as Fig. S13, lines 378–402, pages 24–25). We clarified that the spectra in Fig. 1h and Fig. 3 are normalized by *I*/*V*.

***Comment 2-5.*** *Minor suggestion: it would be interesting to carry out spin-polarized DFT+U calculations, which can count better for e-e correlation than standard GGA PBE calculation at roughly similar computational cost.*

**Response 2-5:** We thank the Reviewer for raising this issue. We are sorry for the omission of methodological details, including the specific approach used in DFT+*U* calculations and the chosen *U* value, in the Methods section. To account for electron-electron (Hubbard *U*) interactions, we indeed performed DFT+*U* calculations with various *U* values (see original Fig. S6). By comparing the calculated density of states (DOS) the experimentally observed peak positions and spectral features, we determined a suitable on-site Hubbard $U = 0.5$ eV for considering Coulomb interactions. We regret not explicitly mentioning it in the methods section, despite it being discussed in lines 168-169 on page 8 of the original manuscript.

**Action 2-5:** Complying with *Com0ment 2-1*, we have added the description of the spin-polarized DFT+*U* calculations in the Methods section (lines 397–398, page 19 in the main text).

***Comment 2-6.*** *In DFT simulations, was the graphene substrate considered? What is the interaction of MoTe layer with the substrate (see also Q3)?*

**Response 2-6:** We sincerely thank the Reviewer for this insightful question. In our DFT calculations, the graphene substrate was not directly included in our models. The choice of this simplified model was based on the following consideration regarding the potential effects of $Mo_{33}Te_{56}$-graphene interactions.

1) **Interfacial charge transfer**: To assess this effect, we conducted preliminary calculations for $Mo_{33}Te_{56}$-interface heterostructure with a rotational angle of 0º. The results indicate a neglectable charge transfer of approximately 0.25 *e*/supercell (< 0.01 *e*/Mo), which keeps the kagome band structures of $Mo_{33}Te_{56}$ intact. A similarly small value was also reported for interactions between graphene and single-layer chalcogenides, as noted in previous work [*Nat. Commun.* **15**, 8056 (2024); *RSC Adv.* **13**, 2903−2911 (2023); *Phys. Rev. B Condens. Matter* **83**, 235411 (2011)].

2) **In-plane stain**: Our experimental observations reveal that the $Mo_{33}Te_{56}$ monolayers exhibit randomly distributed twist angles with respect to the graphene substrate. This randomness suggests that no epitaxial relationship is established (see revised Fig. S2a-d), making it unlikely for the graphene substrate to induce significant in-plane strain on the $Mo_{33}Te_{56}$ layers.

3) **Dielectric screening**: The screening effect introduced by the graphene substrate can be approximated by adjusting the effective on-site Hubbard *U* value in our calculations. We found that setting $U = 0.5$ eV successfully reproduces the experimental results (Fig. S7b, g), effectively capturing the screening effect without the need for explicit graphene.

The parent state of $Mo_{33}Te_{56}$ exhibits a high density of states at the Fermi level, a feature that remains largely unaffected by these substrate-related effects. As a result, the key electronic properties discussed in our work, namely electron correlations and spin polarization arising from the partially filled kagome bands, are robust regardless of the presence of graphene. Additionally, incorporating graphene explicitly in our DFT simulations would be computationally demanding and inefficient for the scope of this study. While substrate effects on electron-electron correlations present an interesting avenue for future exploration, a systematic theoretical and experimental investigation

would be required to fully elucidate such effects.

**Action 2-6:** We have clarified that the calculations do not include the graphene substrate (lines 409–413, page 20 in the Methods section) and have added relevant text to explain that the discussion based on substrate-free calculations is justified (lines 210–230, pages 13–14 in SI).

*Reviewer #3 (Remarks to the Author):*

***Comment 3-0.*** *The paper reports the experimental realization of kagome physics in a new monolayer Mo-Te stoichiometric phase, $Mo_{33}Te_{56}$, synthesized through molecular beam epitaxy. It demonstrates the manifestation of both ferromagnetism and correlated insulating states. The authors employed a combination of experimental techniques (MBE, STM, SP-STM, AFM, etc.) alongside theoretical methods (DFT, TB, group theoretical analysis, etc.). The results are coherent and well-aligned, showing an innovative and robust approach to constructing novel kagome structure within atomically thin van der Waals materials. I believe this paper is worthy of consideration for publication in Nature Communications. There are some minor comments:*

**Response 3-0:** We sincerely thank the Reviewer for their meticulous review and valuable recommendation. We have addressed his/her insightful comments in detail in the following point-by-point responses.

***Comment 3-1.*** *Fig. 1b&c exhibits chiral "wagon-wheel-like" structures, whereas the kagome lattice is typically characterized by in-plane mirror symmetry. How can these chiral structures be reconciled with the kagome lattice framework? Could the authors provide a more schematic explanation to clarify this?*

**Response 3-1:** We thank the Reviewer for this constructive suggestion. A classic kagome lattice, consisting of two corner-shared triangles of identical size, has mirror symmetry in both the *x* and *y* directions. Meanwhile, the wagon-wheel structures (Fig. 1b&c) indeed exhibit chiral structures without in-plane mirror symmetry. We make a brief interpretation below to resolve this “paradox”.

1) First, the kagome lattice can have mirror symmetry broken via certain types of distortion, while the flatness of electronic bands is primarily maintained. A widely studied example is the breathing kagome (left panel of Fig. R7a), where the two triangles are not identical in size, and the mirror symmetry is partially broken (*w.r.t.* the *y* direction). By further tilting the two unequal triangles (right panel of Fig. R7a), we illustrate that the mirror symmetry can be removed entirely.

2) Fig. R7a shows a schematic diagram illustrating the possibility of breaking mirror symmetry in the kagome lattice. The actual situation in our experimental system might be more complex.

Although the real-space grid of the TB model in Fig. R7b seems to be mirror symmetry preserved, the effective electronic kagome lattice (schematically shown in Fig. R7c) shows the complete breaking of mirror symmetries, attributed to the large discrepancy in the hopping energies in different directions (*i.e.*, $t_p$ and $t_a$) and the in-plane chiral charge density distribution (CDD). Note that the TB simulation here only presents a theoretical possibility. Extra effort with a combination of multifold experimental/theoretical techniques is needed to thoroughly address the chirality in the effective electronic kagome lattice.

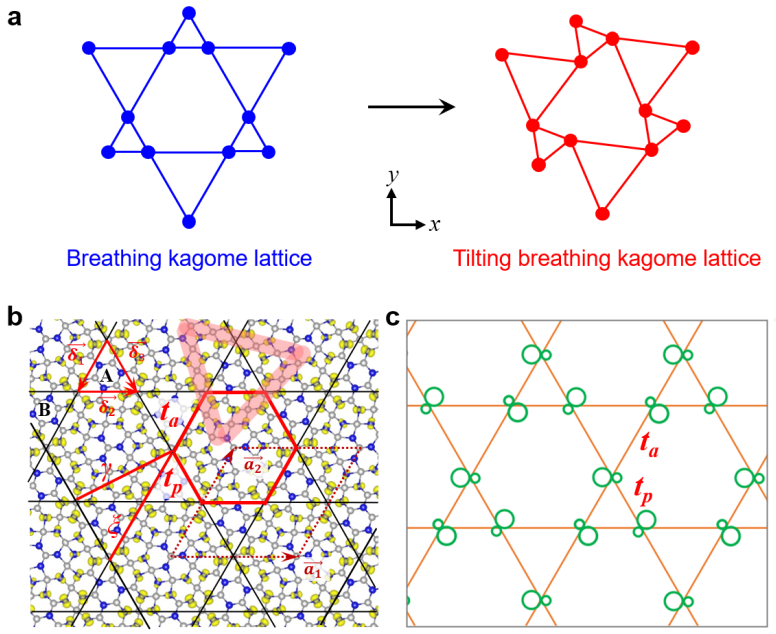


**Fig. R7. a**, Schematics of the breathing kagome lattice (left panel) and tilting breathing kagome lattice (right panel). **b**, Atomic model of the MTB superlattice with a charge density distribution for Γ2 states (for details, see Supplementary Note 2). The charge density orbital profiles are used as the basis in the tight-binding simulation of the kagome lattice (drawn by the black lines). The nearest-neighbour hopping strengths are marked as $t_p$ and $t_a$. The wine-red rhombus indicates a supercell of the breathing kagome lattice. The pink shadow regions depict the boundaries. The breaking of mirror symmetry cannot be visualized in **b**. Here, we display a schematic for the effective electronic kagome lattices (orange lines) in **c**. The lattice lengths are plotted according to the hopping strengths (*i.e.*, $t_p$ and $t_a$), manifesting a notable appearance of a breathing kagome lattice. In addition, the CDD in **b** has a chiral symmetry resulting from the chiral atomic structure. The green profiles with asymmetric dumbbell outlines are used to present the chiral basis orbitals.

**Action 3-1:** In the resubmitted files, we have expanded the discussion on chirality in the SI (lines 244–250, page 15).

***Comment 3-2.*** *The authors provide a fairly comprehensive analysis of the gap formation mechanism at the Fermi level, particularly in their exclusion of specific manifestations of a Coulomb gap, such as V-shaped gaps or those arising from Coulomb blockade. However, it is worth noting that the possibility of a Coulomb gap could persist in the absence of these effects. For example, previous studies have shown that U-shaped gaps can emerge due to tunneling into Landau levels, which are a characteristic signature of topologically flat bands, independent of band filling [Phys. Rev. Lett. 69, 3804–3807 (1992); Nature 464, 566–570 (2010)]. It might be beneficial for the authors to consider these potential scenarios in their analysis.*

**Response 3-2:** We thank the reviewer for highlighting the interesting mechanism that could cause a U-shaped gap resulting from the Coulomb effect. According to this scenario, "the electrons are treated as classical point charges at fixed positions in space with no overlap of the electronic wave functions" [*Phys. Rev. Lett.* **79**, 2867 (1997)]. Consequently, a minimum energy ($E$c ~ $e^2/\varepsilon l_b$) is required for electron tunneling between Landau orbitals. Here, $l_b$ is the magnetic length (*i.e.*, the localization length), which varies from 10 to 100 nm within the experimental $B$ range. In our system, the overlap of wavefunctions (*i.e.*, inter-site hopping) is an important feature of the kagome materials. This overlap (or hopping) leads to the presence of flat and Dirac bands, indicating no significant localization on the length scale of Landau orbitals observed in graphene systems. Therefore, we consider it less likely that this picture is the cause of the gap we observe. Even considering the gap mechanism proposed by the reviewer, it remains "a correlation effect of electrons in a nearly flat band" [*Phys. Rev. Lett.* **69**, 3804–3807 (1992)], which does not contradict our major conclusion. Our primary finding is that the observed gap at the Fermi level is due to electron correlation effects, resulting in a correlated insulating state rather than a band insulator. In our original manuscript (lines 308–310, page 14) and the revised SI (lines 514–516, page 31), we

have explicitly clarified the term "correlated insulating states" to ensure clarity and avoid any potential misunderstanding.

We agree with the Reviewer's comment that a continuous tunneling of the electron density is an important approach to thoroughly understand the material and reveal its more potential value. However, it is beyond the scope of the present study, which aims to fabricate and demonstrate the first example of a crystalline single-layer kagome crystal with emergent properties driven by kagome bands.

**Action 3-2:** In the resubmitted files, we have revised and included more detailed discussion of the correlated gap in our system (lines 504–509, page 31 in SI).

***Comment 3-3.*** *The gap size mentioned in the manuscript is 15 mV. How was this value determined from the tunneling spectra? Was spatial variation taken into account when reporting this number? If it's a statistical average, an error bar should be included.*

**Response 3-3:** We thank the Reviewer for raising this important question. To assess the spatial uniformity of the gap within a supercell, we recorded multiple high-resolution d$I$/d$V$ spectra at $T$ = 0.35 K from representative sites, including the $TD_{E/U}$ and centre sites. As shown in Fig. R8a (4a), these spectra consistently exhibit a relatively uniform hard gap. To further validate this result, we also measured d$I$/d$V$ spectra (centre site) across multiple islands with varying sizes, ranging from 38 nm² to 2867 nm². As depicted in Fig. R8b (S16b), all spectra exhibit a similar hard gap, a comparable gap size of approximately 15 meV, regardless of the island size.

In compliance with the Reviewer's suggestion, we conducted a more rigorous statistical analysis, as shown in Fig. R8c. Measurements were randomly taken from various islands over the sample surface. While local structural variations (such as defects) may contribute to some deviations, the Gaussian fitting of the gap histogram yields a statistical result of $\Delta_0 = 15.23 \pm 1.86$ mV.

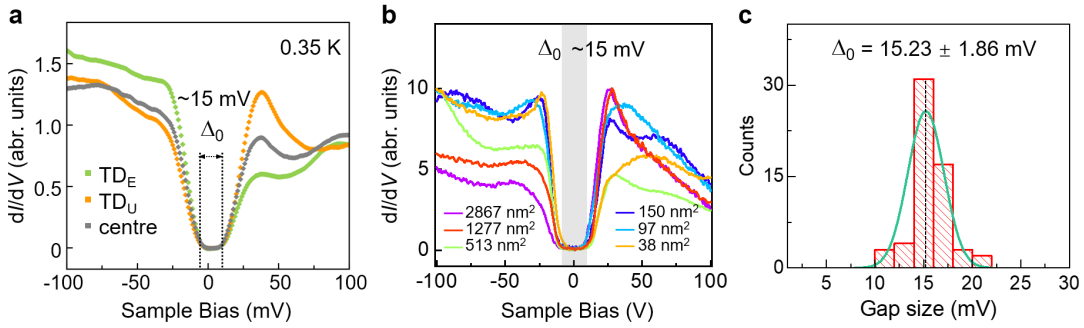


**Fig. R8. a**, High-resolution d$I$/d$V$ spectra recorded at the $TD_{E/U}$ and centre sites at $T$ = 0.35 K within one supercell, showing a relatively uniform hard energy gap. $\Delta_0$ denotes the size of the zero-conductance region. **b**, d$I$/d$V$ spectra measured at centre site on different islands with areas ranging from 38 nm$^2$ to 2867 nm$^2$. All measurements exhibit a hard gap with nearly identical gap size ($\Delta_0$ ~ 15 meV) regardless of the island size. **c**, Statistical analysis of the gap sizes. The green line is the fitting distribution curve which indicates an average value ($\Delta_0$ = 15.23 ± 1.86 mV).

**Action 2-4:** We have revised the gap size value as 15.23 ± 1.86 mV (lines 302–303, page 14 in the main text). Additionally, we have added the statistical analysis in Fig. S16 of the revised SI, now labelled as Fig. S16c (lines 457–461, page 29).

***Comment 3-4.*** *The authors mention that the $Mo_{33}Te_{56}$ phase is uniform across nearly the entire sample. It would be better if additional evidence could be provided to support this claim.*

**Response 3-4:** We thank the Reviewer for raising this concern. In the revised Fig. S1 (also present in Fig. R9), we present quite a few large-scale images taken at random sample locations. In all images, the superlattice with a uniform 1.91-nm periodicity is observed as an overwhelming majority. In addition, the $Mo_{33}Te_{55}$ phase can be well separated from other Mo-Te phases with optimized growth parameters. As seen in Fig. S1, only the $Mo_6Te_6$ wires appear at the very edge of 2D flakes; all other ones (e.g., MTBs with different sizes, $Mo_5Te_8$, $MoTe_2$) are absent in these samples. This indicates the relative thermal preference of the $Mo_{33}Te_{56}$ phase, and there shall be an accessible growth window to prepare the scalable $Mo_{33}Te_{56}$ sample. Our recent work [*Appl. Phys. Lett.* **125**, 151601 (2024)] provides additional technical details on the growth processes that convincingly demonstrate the uniformity of the $Mo_{33}Te_{56}$ phase.

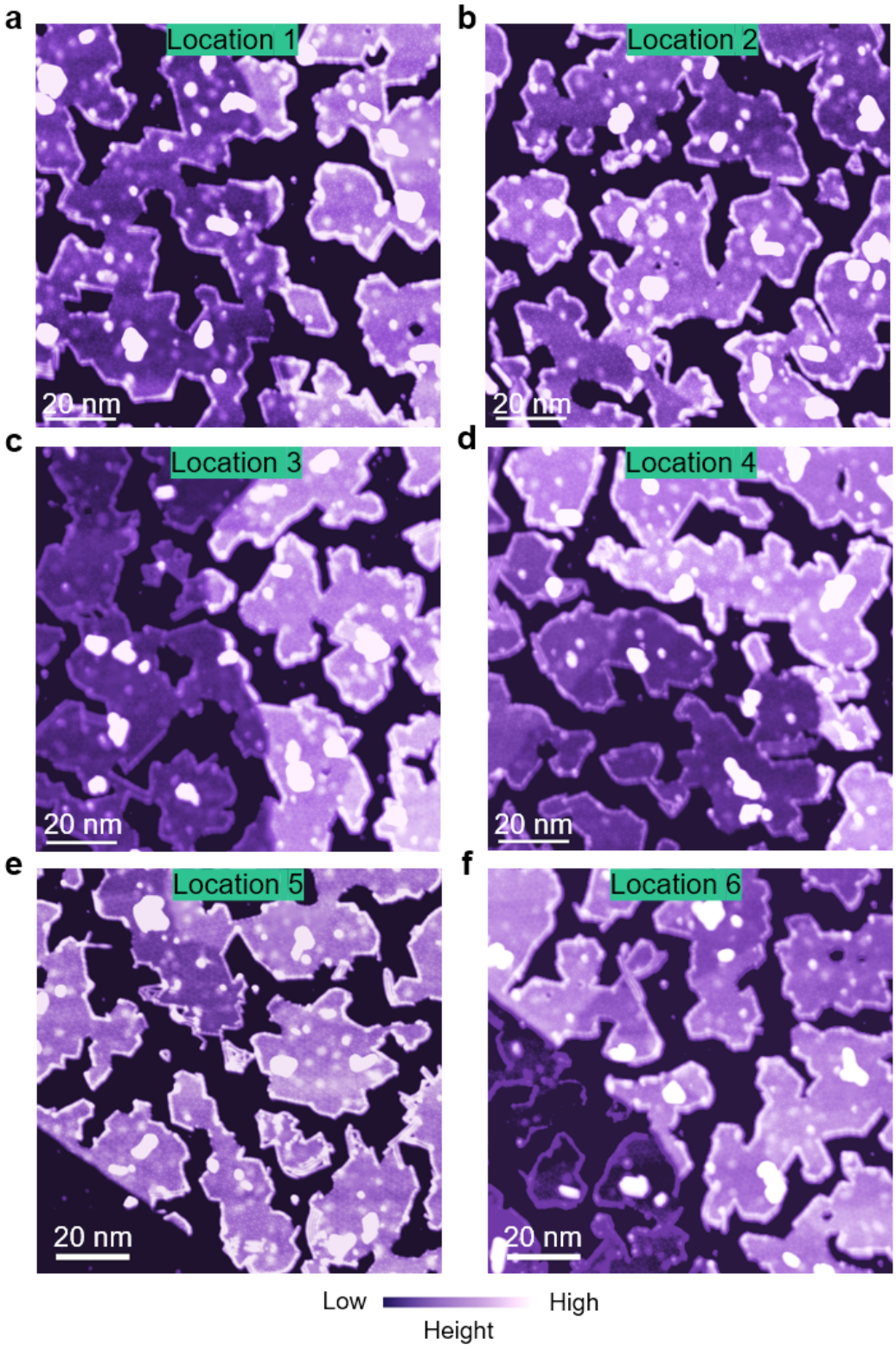


**Fig. R9 (S1). a-f**, High-resolution STM images of monolayer $MoTe_{2-x}$ acquired at six random locations on an as-grown sample [see preparation recipe in the Methods section]. We used the coarse motion motor to ensure large separations (at least by hundreds of micrometers) among these six locations. The 1.91-nm MTB superlattice is the dominant phase in all images (> 90 %). The bright spots are amorphous residuals on top of ML-$MoTe_{2-x}$, and the $Mo_6Te_6$ wires start to appear at the flake edges. Scanning parameters: $V_{bias}$ = 0.8 V, $I_t$ = 20 pA; size: 120 × 120 $nm^2$.

**Action 3-4:** We have incorporated the above-mentioned Fig. R9 and the corresponding discussion in the revised Supporting Information (now designated as Fig. S1) and referenced it in the main text (lines 87–88, page 4).

***Comment 3-5.*** *In Fig. S5e, the dI/dV spectra show the in-gap states for N = 3, 4, 5. Are there any further experimental/theoretical investigations on the morphology and electronic structure of these states? Do they still exhibit the kagome band properties?*

**Response 3-5:** We thank the Reviewer for this inspirational comment. Our DFT calculations show that the formation energies of the $N = 4$ (pink line) and 5 (green line) phases are more favorable under Te-rich conditions (Fig. R10a) [*arXiv:* 2408.14285]. Experimental observations of $N = 4$ and 5 were usually achieved at lower substrate temperatures than required for $N = 3$ (*i.e.*, $Mo_{33}Te_{56}$), as detailed in our recent work [*Appl. Phys. Lett.* **125**, 151601 (2024)]. However, these phases are more locally ordered with very limited coverage across the sample. The STM topography images shown in Fig. R10b confirm their structure, which resembles the primary focus of this work but with an enlarged size, where each triangular domain is composed of 4 or 5 Te atoms along each edge (as shown in Fig. S6b and the inset of Fig. R10b). Regarding the electronic structure, our theoretical calculations have provided a systematic and detailed study of these phases [*arXiv:* 2408.14285]. Specifically, the DFT-calculated band structure of the $N = 4$ monolayer reveals two sets of kagome bands, as indicated by the blue and red lines in Fig. R10c. Further theoretical investigations demonstrate that Mo-Te monolayers, with varying sizes and MTB loop arrangements, exhibit diverse magnetic properties, as summarized in Fig. R10d. To avoid confusion, we have used colourful shadows in Fig. R10d to highlight the following: the $N = 3$ phase exhibits magnetic behaviour (the blue shadow), as confirmed by our experimental work, while the $N = 4$ and $N = 5$ phases exhibit non-magnetic characteristics (pink and green shadows, respectively). However, further exploration is required for the experimental characterization of the magnetic structures of these two phases.

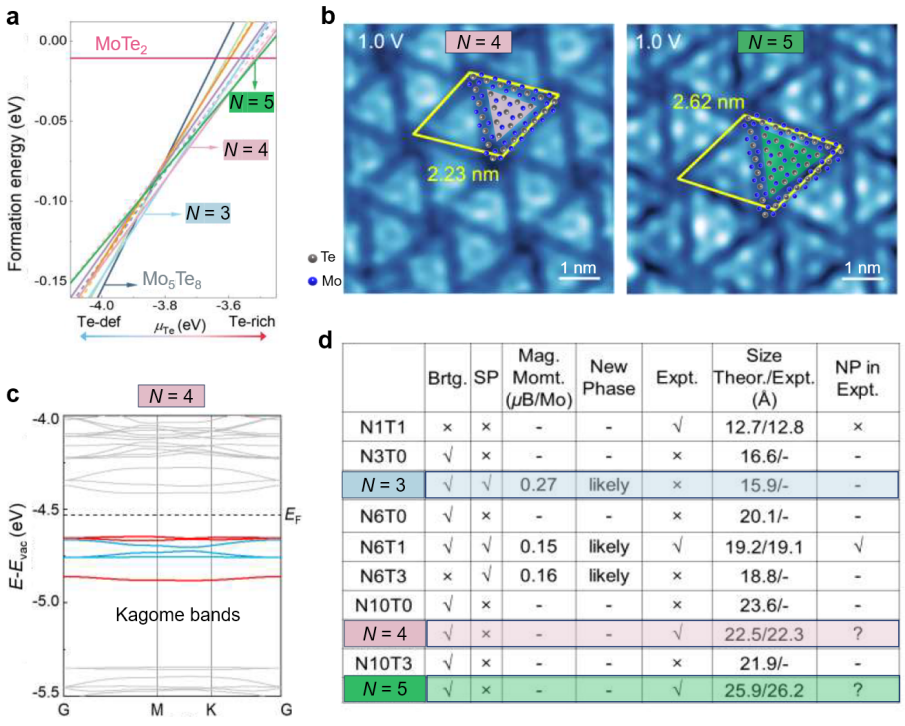


| | Brtg. | SP | Mag. Momt. (μB/Mo) | New Phase | Expt. | Size Theor./Expt. (Å) | NP in Expt. |
|---|---|---|---|---|---|---|---|
| N1T1 | × | × | - | - | √ | 12.7/12.8 | × |
| N3T0 | √ | × | - | - | × | 16.6/- | - |
| *N* = 3 | √ | √ | 0.27 | likely | × | 15.9/- | - |
| N6T0 | √ | × | - | - | × | 20.1/- | - |
| N6T1 | √ | √ | 0.15 | likely | √ | 19.2/19.1 | √ |
| N6T3 | × | √ | 0.16 | likely | × | 18.8/- | - |
| N10T0 | √ | × | - | - | × | 23.6/- | - |
| *N* = 4 | √ | × | - | - | √ | 22.5/22.3 | ? |
| N10T3 | √ | × | - | - | × | 21.9/- | - |
| *N* = 5 | √ | × | - | - | √ | 25.9/26.2 | ? |

**Fig. R10. a**, Formation energies of different monolayer Mo-Te phases, with blue, pink, and green squares highlighting $N$ = 3, 4, and 5, respectively. It is noted that the definition of "$N$" in this theoretical work [*arXiv:* 2408.14285] differs from that in our current study, where it refers to the number of $Te_2$ dimers within the triangular domain encircled by the MTB loop. In Fig. R10 and the above discussion, we have adjusted the markers in the theoretical figures according to the definition in the present work to ensure consistency. **b**, STM topography images of $N$ = 4 and 5, measured at a bias voltage of 1.0 V. Insets display the corresponding atomic models, with $N$ denoting the number of Te atoms at the domain (*i.e.*, the pink and green triangles) edges. **c**, DFT-calculated band structures of the $N$ = 4 monolayer, with the kagome bands indicated by the blue and red lines. **d**, Different categories for all configurations distinguished by size, symmetry, and magnetization in theory (*Theor.*) and experiment (*Expt.*) [*arXiv*: 2408.14285].

***Comment 3-6.*** *The authors should consider adding graphical representations to make the kagome lattice more visually intuitive and comprehensible.*

**Response & Action 3-6:** We thank the Reviewer for this suggestion. Complying with the *Comment 1-3*, we have added the kagome pattern lines in revised Fig. 2c.

***Comment 3-7.*** *In Fig. 4a, the caption "$TD_{A/B}$" should be revise to "$TD_{E/U}$" for consistency with the manuscript.*

**Response & Action 3-7:** We are sorry for the oversight. The correct label should indeed be "$TD_{E/U}$". We have corrected the caption in the revised Fig. 4a.

*Reviewer #4 (Remarks to the Author):*

***Comment 4-0.*** *I co-reviewed this manuscript with one of the reviewers who provided the listed reports. This is part of the Nature Communications initiative to facilitate training in peer review and to provide appropriate recognition for Early Career Researchers who co-review manuscripts.*

**Response 4-0:** We thank the Reviewer for his/her careful review, constructive comments, and positive recommendation. We have carefully considered all the feedback provided and have incorporated the suggested revisions into our manuscript. We believe these adjustments have improved the quality and clarity of the work.

# Point-by-point responses to reviewer comments

Manuscript ID: NCOMMS-24-78805A

Title: "*Ferromagnetism and correlated insulating states in monolayer $Mo_{33}Te_{56}$*"

*Reviewer #3 (Remarks to the Author):*

***Comment 3-0.*** *The authors have answered all of the comments very well, I think it can be accepted for publishing. Before that, a few minor issues need to be considered.*

**Response 3-0:** We sincerely appreciate the Reviewer for his/her recommendation of publication. We addressed his/her comments in the following and improved the manuscript accordingly.

***Comment 3-1.*** *In page 6 line 142, the author claim "In contrast, the present pattern exhibits uniformity across nearly the entire sample.". Since STM and AFM characterization is locally in a small region, such claim is a little bite of over optimistic, unless the author present some evidence from macroscopic measurement, such as LEED pattern. And also such $Mo_{33}Te_{56}$ phase is special stoichiometric Mo-Te compounds that form via an annealing process of the single-layer H-$MoTe_2$, I doubt it can be uniformly cover the entire sample. I suggest the author tune down a little.*

**Response & Action 3-1:** We greatly thank the Reviewer for this suggestion. We acknowledge that STM and AFM are local characterization techniques, and that macroscopic evidence (*e.g.*, LEED patterns) would indeed strengthen the argument regarding uniformity. However, due to the random distribution of sample orientations, we were unable to obtain high-quality electron diffraction patterns. We have refined the wording to provide a more appropriate description. The revised sentence now reads: "*In contrast, the present pattern exhibits a high degree of uniformity across the extensively characterized regions of the sample.*" (lines 142–144, page 6 in the main text).

***Comment 3-2.*** *In figure 1g caption, they state "the dI/dV spectra are normalized by the*

*total conductance (I/V) to mitigate the influence of bias-dependent tunneling probability on the spectral weight." So all STS panels should be lableled as "(dI/dV)/(I/V)", instead of "normalized dI/dV" or "dI/dV". please correct it.*

**Response & Action 3-2:** We greatly thank the Reviewer for this suggestion. We have corrected the labels to "(d$I$/d$V$)/($I$/$V$)" accordingly to ensure consistency throughout the manuscript. The modifications have been applied to Fig. 1h and Fig. 3b in the main text as well as Fig. 12a and Fig. 13b in the Supplementary Information.

***Comment 3-3.*** *Although the author use a large paragraph in Supplementary Information (SI) to describe how "The array of MTB loop triangles forms a breathing colouring-triangle pattern.", it is still hard to see the Kagome structure. I suggest the author can draw accordingly the Kagome lattice in Fig. 1 or Fig. 2.*

**Response & Action 3-3:** We appreciate the Reviewer's insightful suggestion. We have already added the kagome pattern lines in Fig. 2c with the lattice points at the boundary centre (lines 214–215, page 9 in the main text). This provides a clear and intuitive schematic representation of the kagome geometry in real space.